Electronic Supplementary Material (ESI) for Journal of Materials Chemistry A.
This journal is © The Royal Society of Chemistry 2023

Electronic Supplementary Information (ESI)

Overall water electrolysis on graphdiyne-iron oxyhydroxide heterostructure

Xi Chen,[ac] Danyan Zhang,[ac] Xuchen Zheng,[ac] Chao Zhang,[ac] Yang Gao,[a] Chengyu Xing,[a] Siao Chen,[ac] Han Wu,[ac] Yurui Xue *[ab] and Yuliang Li *[ac]

[a]*CAS Key Laboratory of Organic Solids, Institute of Chemistry, Chinese Academy of Sciences, Beijing 100190, China. E-mail: ylli@iccas.ac.cn*

[b]*Shandong Provincial Key Laboratory for Science of Material Creation and Energy Conversion, Science Center for Material Creation and Energy Conversion, School of Chemistry and Chemical Engineering, Shandong University, Jinan 250100, China. E-mail: yrxue@sdu.edu.cn*

[c]*University of Chinese Academy of Sciences, Beijing 100049, China*

*Corresponding author. E-mail: Yurui Xue, yrxue@sdu.edu.cn; Yuliang Li, ylli@iccas.ac.cn

Experimental Section

Chemicals and materials

$FeCl_3 \cdot 6H_2O$ was brought from Energy Chemical. Anhydrous Na_2SO_4, tetrabutylammonium fluoride, and hexabromobenzene were provided by Beijing Chemical Works, Alfa Aesar, and J&K Scientific respectively. Toluene, ethyl acetate, dichloromethane, acetone, pyridine, N, N-dimethylformamide (DMF), and tetrahydrofuran (THF) were purchased from Tianjin Concord Technology Co., Ltd. Toluene and THF were refluxed with sodium crumbs to remove water. The water used in all experiments was purified with a Millipore system and the other reagents were directly used without any purification unless specifically mentioned.

Synthesis of FeOOH nanowires electrode

FeOOH nanowires electrode was synthesized through a facile treatment. Firstly, 70 mL aqueous solution containing 3.0 mM $FeCl_3$ and 4.8 mM Na_2SO_4 was vigorously stirred until the solution became clear. A piece of cleaned carbon cloth (CC, 4 cm × 6 cm) was next added into the homogeneous solution and the whole system was heated to 120 ˚C and kept for 6 h. After the reaction, the obtained FeOOH nanowires/CC electrode was taken out and washed with distilled water and acetone, and dried naturally in ambient conditions.

Synthesis of FeOOH@GDY electrode

FeOOH@GDY electrode was synthesized by in-situ growth of GDY on the surface of FeOOH nanowires through a typical cross-coupling reaction at room temperatures. In brief, FeOOH nanowires/CC electrode was directly used as the substrate and put into the reaction flask containing 10 mL ethyl acetate of hexakis[(trimethylsilyl)-ethynyl]benzene (HEB, 1.0 mg mL^{-1}), 10 mL dichloromethane, and 2 mL pyridine. The whole system was kept at 60 ˚C for 3 days. After the reaction, the as-prepared FeOOH@GDY electrode was taken out and washed with DMF and acetone several times to remove residual impurities and dried naturally for characterizations and electrochemical measurements.

Material Characterizations

S−4800 field emission scanning electron microscope was used to obtain scanning electron microscopy (SEM) images. Transmission electron microscopy (TEM), high-resolution transmission electron microscopy (HRTEM) images, and elemental mapping results were

collected through JEM−2100F electron microscope. XRD results were obtained by conducting X−ray diffraction on a Japan Rigaku D/max−2500 rotation anode X-ray diffractometer using Cu Kα radiation (λ=0.15418 nm). X-ray photoelectron spectroscope (XPS) measurements were performed by using Thermo Scientific ESCALab 250Xi instrument with monochromatic Al Kα X-ray radiation. Raman spectra were obtained using a Renishaw−2000 Raman spectrometer with a 473 nm excitation laser source. The infrared (IR) spectra were recorded at a resolution of 2 cm^{-1} on a Bruker Vertex 70v vacuum micro-Fourier infrared spectrometer, scanning from 4000 to 400 cm^{-1} at room temperature.

Electrochemical measurements

All electrochemical measurements were performed using an electrochemical workstation (CHI660E, Shanghai CH. Instruments, China) with a typical three-electrode system, where the saturated calomel electrode (SCE) was utilized as the reference electrode, the graphite rod as the counter electrode and the freshly-prepared samples as the working electrode. The potentials reported in this work were converted to the reversible hydrogen electrode (RHE) scale via calibration with the following equation: E(RHE) = E(SCE) + 0.242 + 0.0591 × pH, and the presented current density was obtained from the geometric surface area (about 4 × 2.5 mm). HER, OER, and OWS activities were tested by linear sweep voltammetry (LSV) measurements in 1.0 M H_2-saturated and O_2-saturated KOH electrolytes, respectively, with a scan rate of 2 mV s^{-1}. The sweep rate of the cyclic voltammetric (CV) curve test was 100 mV s^{-1}. The double-layer capacitance (C_{dl}) values of the catalysts were measured through cyclic voltammetry (CV) method in a non-Faradaic region (0.05 V − 0.15 V *vs.* SCE) at different scan rates (20, 40, 60, 80, 100, and 120 mV s^{-1}). The long-term stability tests of the catalysts were carried out using the chronoamperometric method under constant overpotential. Under open circuit voltage, the frequency range of electrochemical impedance spectroscopy (EIS) measurements was 0.01 to 100000 Hz. Tafel plots of potential (V) *vs.* log(j) were recorded with a linear portion of LSV curves at low potential fitted to the Tafel equation:

$$\eta = b \log j + a$$

where η is overpotential, j is the current density and b is the Tafel slope.

Supplementary Figures

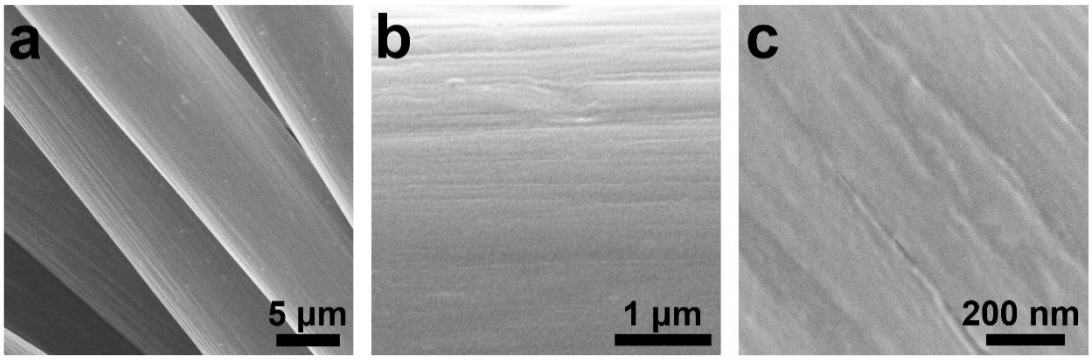

Fig. S1. The low- and high-resolution SEM images of CC.

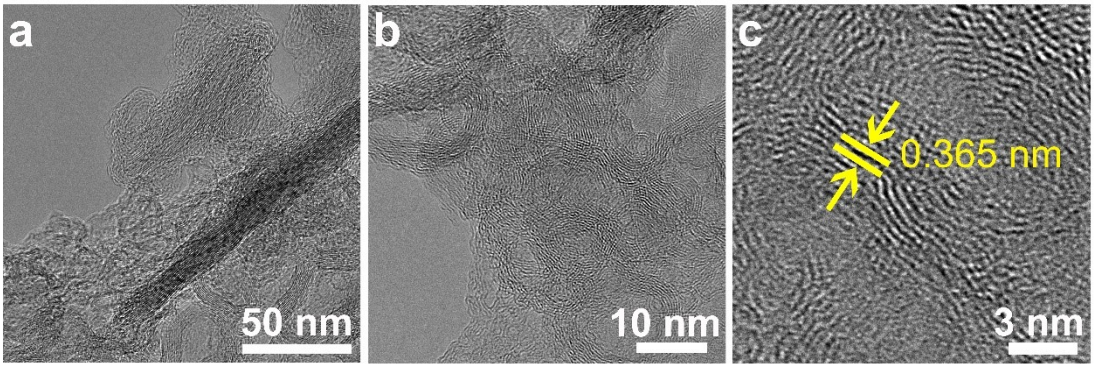

Fig. S2. The low- and high-resolution TEM images of pure GDY.

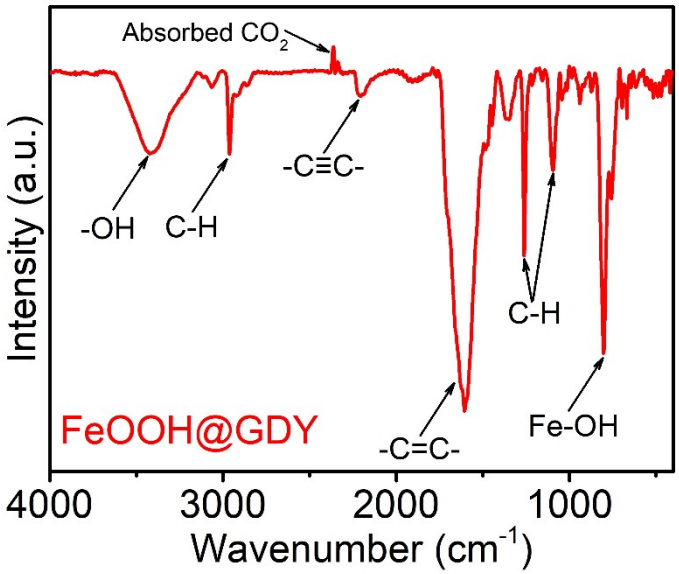

Fig. S3. The IR spectroscopy of FeOOH@GDY.

−OH groups are found in the IR spectrum of FeOOH@GDY. The adsorption peak at 3420 cm^{-1} is the −OH stretching vibrations of physically absorbed H_2O and structural OH^- groups of FeOOH. The peak at 799 cm^{-1} could be assigned to Fe−OH bending vibrations. The band at 669 cm^{-1} is attributed to Fe−O and Fe−OH stretching. These −OH groups are favorable for the adsorption of intermediates during the reaction process. The peaks at 2959, 1261 and 1095 cm^{-1} (C−H), 2206 cm^{-1} (−C≡C−), and 1601 cm^{-1} (aromatic ring) proves the existence of GDY.

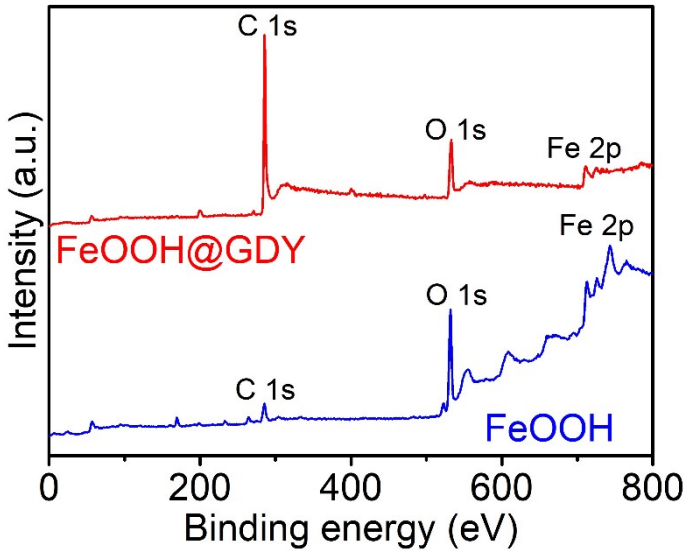

Fig. S4. XPS survey spectra of FeOOH and FeOOH@GDY.

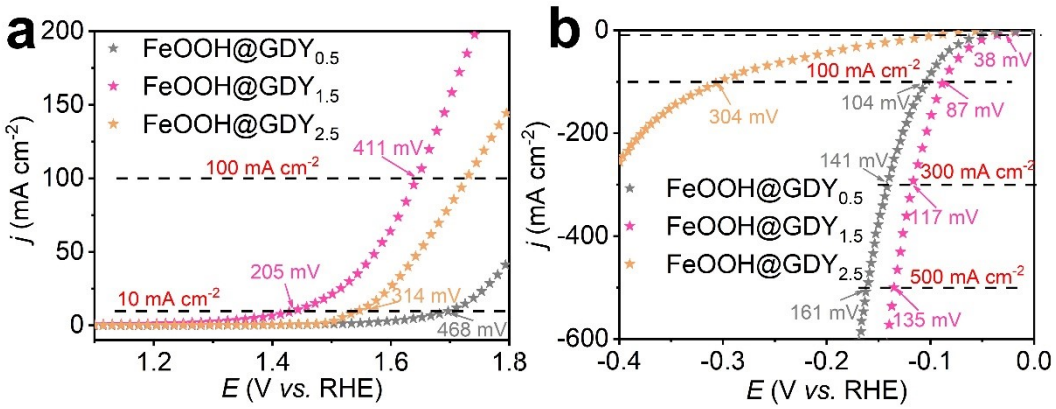

Fig. S5. (a) OER performance and (b) HER performance of FeOOH@GDY with different GDY contents.

The content of GDY in the composites was measured to be 1.5 mg cm^{-2}. Samples with different GDY contents have been synthesized and denoted as $FeOOH@GDY_{0.5}$, $FeOOH@GDY_{1.5}$, and FeOOH@GDY-$_{2.5}$, respectively. As shown in **Fig. S5**, the $FeOOH@GDY_{1.5}$ has the excellent OER and HER performance with the overpotential of 205 and 38 mV at the current density of 10 mA cm^{-2}, better than that of both $FeOOH@GDY_{0.5}$, and $FeOOH@GDY_{2.5}$.

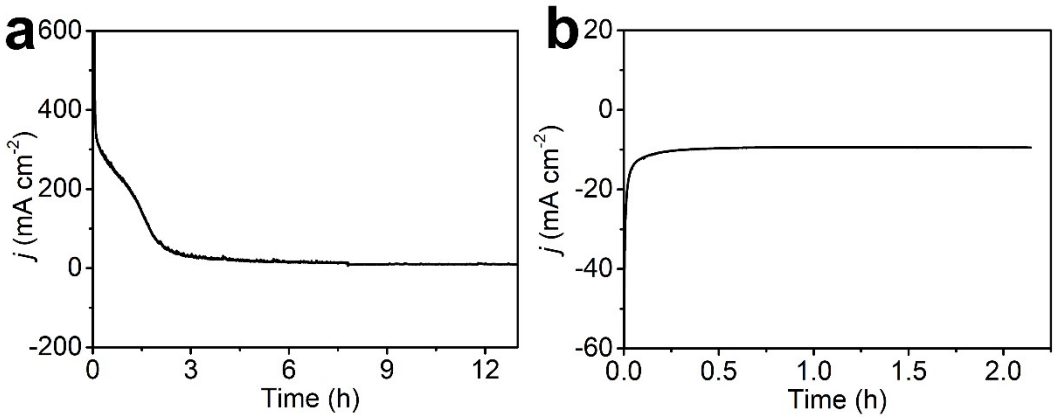

Fig. S6. The time-dependent current density curves of (a) OER and (b) HER of FeOOH.

As shown in **Fig. S6**, FeOOH showed obvious decrease in the current densities for both OER and HER processes even at the beginning of the stability tests. These results further demonstrated the important role of GDY in enhancing the stability of the catalysts.

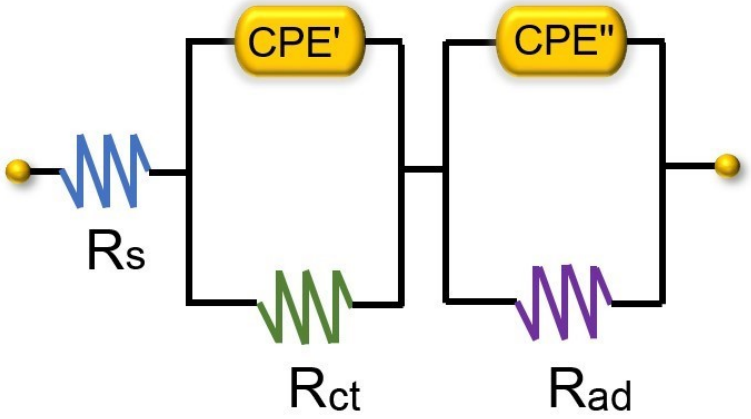

Fig. S7. The equivalent model for EIS data fitting.

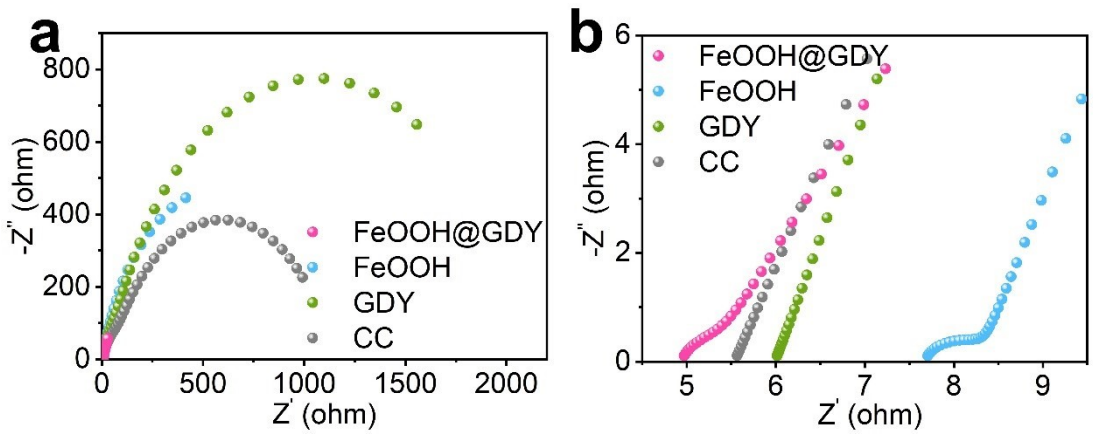

Fig. S8. Simulated Nyquist plots of FeOOH@GDY and controls in 1.0 M KOH.

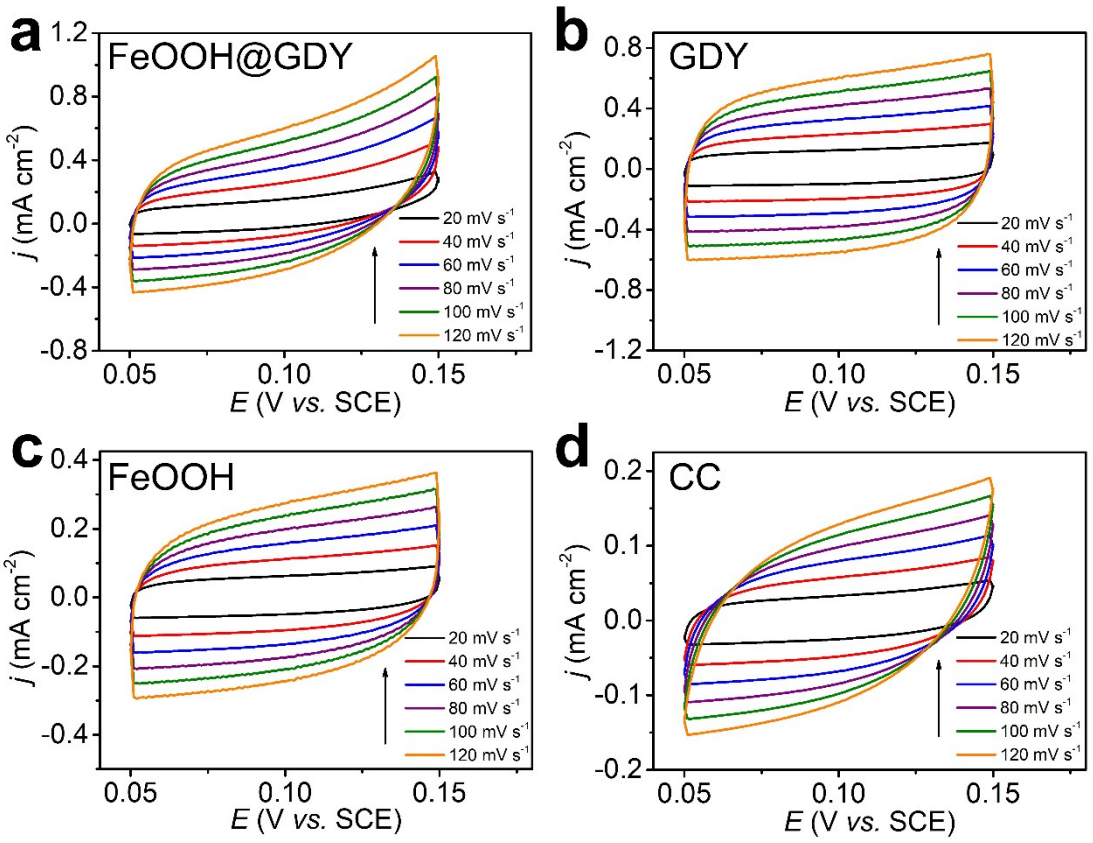

Fig. S9. CV curves of (a) FeOOH@GDY, (b) GDY, (c) FeOOH and (d) CC.

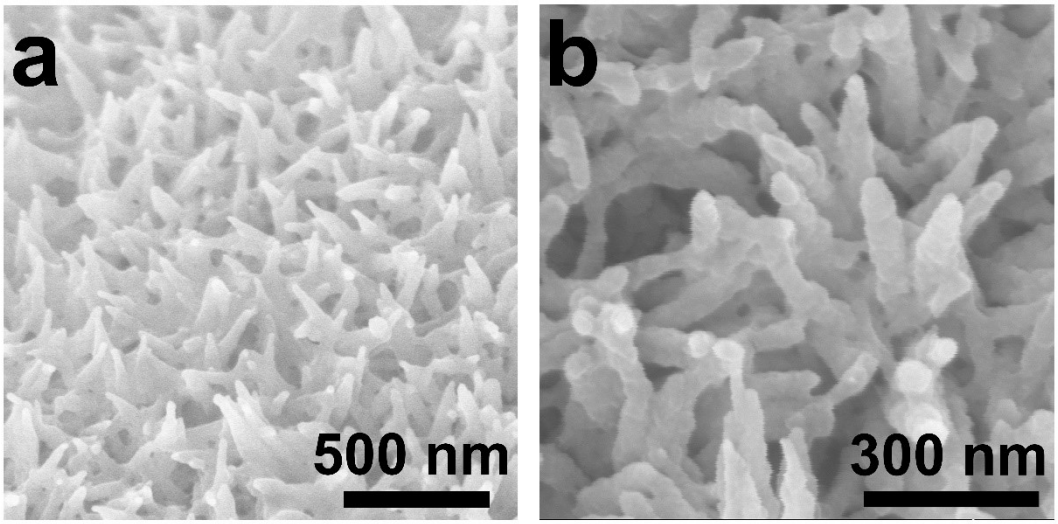

Fig. S10. SEM images of FeOOH@GDY obtained after electrochemical tests.

Supplementary Tables

Table S1. Comparison of FeOOH@GDY with recently reported OER FeOOH-based catalysts under alkaline conditions.

Electrocatalyst	η (mV) @ j=10 mA cm^{-2}	Tafel slope (mV dec^{-1})	Durability (h)	Solution
FeOOH@GDY	205	56	75	1.0 M KOH
FF−Na−Ru[1]	230	46	12	1.0 M KOH
CoP/FeOOH[2]	250	56.6	20	1.0 M KOH
FeOOH@NG[3]	240	42	48	1.0 M KOH
defect-rich FeOOH[4]	307	36	55	1.0 M KOH
γ-FeOOH/NF[5]	286 ± 3	51± 2	24	6.0 M NaOH
S-FeOOH/IF[6]	244	59		1.0 M KOH
ZrNi–FeOOH nanosheets[7]	231			1.0 M KOH
F(V)OOH-1.5[8]	232	30	72	1.0 M KOH
Co@CoFe-NBs[9]	266	26.94	12	1.0 M KOH
$Ni_{1/2}Fe_{1/2}(OH)_2$/CNT[10]	244	41		1.0 M KOH
W, P-FeB[11]	209	39.87	25	1.0 M KOH

Table S2. Comparison of FeOOH@GDY with recently reported HER Fe-based catalysts under alkaline conditions.

Electrocatalyst	η (mV) @ j=10 mA cm^{-2}	Tafel slope (mV dec^{-1})	Durability (h)	Solution
FeOOH@GDY	38	46	441	1.0 M KOH
FF–NaCl–Ir–P[12]	69	87.8	12	1.0 M KOH
ZrNi–FeOOH nanosheets[13]	150	110		1.0 M KOH
Co@CoFe-NBs[14]	104	79	12	1.0 M KOH

Table S3. Impedance parameters derived from the fitting to the equivalent circuit for the impedance spectra recorded in 1.0 M KOH.

catalyst	FeOOH@GDY	FeOOH/CC	GDY	CC
R_s (ohm)	4.929	7.682	5.982	5.49
CPE′, Yo [S-sec^n]	1.61×10^{-4}	1.86×10^{-3}	5.49×10^{-4}	3.73×10^{-4}
n	1	0.856	1	0.786
R_{ct} (ohm)	0.31	1170	37.56	1080
CPE″, Yo [S-sec^n]	1.3×10^{-3}	1.14×10^{-4}	5.01×10^{-4}	1.68×10^{-4}
n	0.781	0.950	0.831	0.94
R_{ad} (ohm)	1088	0.6162	2025	51.71

Table S4. Comparison of FeOOH@GDY with recently reported OWS Fe-based catalysts under alkaline conditions.

Electrocatalyst	*E* (V *vs.* RHE) @ *j*=10 mA cm^{-2}	Stability(h)	Solution
FeOOH@GDY	1.43	>115	1.0 M KOH
FF–NaCl–Ir–P[12]	1.47	50	1.0 M KOH
ZrNi–FeOOH nanosheets[7]	1.63	25	1.0 M KOH
F(V)OOH-1.5[8]	1.51	25	1.0 M KOH
Co@CoFe–P NBs[9]	1.49	60	1.0 M KOH
$Ni_{1/2}Fe_{1/2}(OH)_2$/CNT[10]	1.64	12	1.0 M KOH
$Co(OH)_2$@MXene[13]	1.46	100	1.0 M KOH
NiCoFe LDH/NF[14]	1.56	30	1.0 M KOH

Reference

1 Z. Wu, Y. Zhao, H. Wu, Y. Gao, Z. Chen, W. Jin, J. Wang, T. Ma and L. Wang, *Adv. Funct. Mater.*, 2021, **31**, 2010437.

2 J. Cheng, B. Shen, Y. Song, J. Liu, Q. Ye, M. Mao and Y. Cheng, *Chem. Eng. J.*, 2022, **428**, 131130.

3 K. Wu, F. Chu, Y. Meng, K. Edalati, Q. Gao, W. Li and H.-J. Lin, *J. Mater. Chem. A*,2021, **9**, 12152−12160.

4 Y. Hu, J. Zhou, L. Li, Z. Hu, T. Yuan, C. Jing, R. Liu, S. Xi, H. Jiang, J.-Q. Wang and L. Zhang, *J. Mater. Chem. A*, 2022, **10**, 602−610.

5 K. Wang, H. Du, S. He, L. Liu, K. Yang, J. Sun, Y. Liu, Z. Du, L. Xie, W. Ai and W. Huang, *Adv. Mater.*, 2021, **33**, e2005587.

6 X. Chen, Q. Wang, Y. Cheng, H. Xing, J. Li, X. Zhu, L. Ma, Y. Li and D. Liu, *Adv. Funct. Mater.*, 2022, **32**, 2112674.

7 Y. Yan, J. Liu, K. Huang, J. Qi, L. Qiao, X. Zheng and W. Cai, *J. Mater. Chem. A*, 2021, **9**, 26777−26787.

8 F. N. I. Sari, H.-S. Chen, A. k. Anbalagan, Y.-J. Huang, S.-C. Haw, J.-M. Chen, C.-H. Lee, Y.-H. Su and J.-M. Ting, *Chem. Eng. J.*, 2022, **438**, 135515.

9 Y. Zhao, N. Dongfang, C. A. Triana, C. Huang, R. Erni, W. Wan, J. Li, D. Stoian, L. Pan, P. Zhang, J. Lan, M. Iannuzzi and G. R. Patzke, *Energy Environ. Sci.*, 2022, **15**, 727−739.

10 J. Ge, J. Y. Zheng, J. Zhang, S. Jiang, L. Zhang, H. Wan, L. Wang, W. Ma, Z. Zhou and R. Ma, *J. Mater. Chem. A*, 2021, **9**, 14432−14443.

11 Z. Chen, R. Zheng, M. Graś, W. Wei, G. Lota, H. Chen and B.-J. Ni, *Appl. Catal. B*, 2021, **288**, 120037.

12 Z. Zhao, W. Jin, L. Xu, C. Wang, Y and Zhang, Z, *J. Mater. Chem. A*, 2021, **9**, 12074−12079.

13 L. Li, D. Yu, P. Li, H. Huang, D. Xie, C.-C. Lin, F. Hu, H.-Y. Chen and S. Peng, *Energy Environ. Sci.*, 2021, **14**, 6419−6427.

14 Q. Jia, J. Gao, C. Qiu, L. Dong, Y. Jiang, X. Liu, M. Hong and S. Yang, *Chem. Eng. J.*, 2022, **433**, 134552.